

# Joint Trajectory and Passive Beamforming Design for Intelligent Reflecting Surface-Aided UAV Communications: A Deep Reinforcement Learning Approach

Liang Wang, Kezhi Wang, Cunhua Pan, Wei Xu and Nauman Aslam

**Abstract**—In this paper, the intelligent reflecting surface (IRS)-assisted unmanned aerial vehicle (UAV) communication system is studied, where an UAV is deployed to serve the user equipments (UEs) with the assistance of multiple IRSs mounted on several buildings to enhance the communication quality between UAV and UEs. We aim to maximize the overall weighted data rate and geographical fairness of all the UEs via jointly optimizing the UAV's trajectory and the phase shifts of reflecting elements of IRSs. Since the system is complex and the environment is dynamic, it is challenging to derive low-complexity algorithms by using conventional optimization methods. To address this issue, we first propose a deep Q-network (DQN)-based low-complex solution by discretizing the trajectory and phase shift, which is suitable for practical systems with discrete phase-shift control. Furthermore, we propose a deep deterministic policy gradient (DDPG)-based solution to tackle the case with continuous trajectory and phase shift design. The experimental results prove that the proposed solutions achieve better performance compared to other traditional benchmarks.

**Index Terms**—Deep Reinforcement Learning, UAV communications, Reconfigurable Intelligent Surface, Intelligent Reflecting Surface.

## I. INTRODUCTION

In the fifth-generation (5G) wireless networks and beyond, it is widely envisioned that it will achieve 1000-fold increase in network capacity, accommodate at least 100 billion connected devices and support a number of emerging applications such as virtual reality (VR) and augmented reality (AR). To satisfy this ever-increasing demand, unmanned aerial vehicle (UAV) is regarded as one of the most promising technologies to achieve these ambitious goals. Compared to the traditional communication systems that utilize the terrestrial fixed base stations, UAV-aided communication systems are more cost-effective and likely to achieve better quality of service (QoS) due to its appealing properties of flexible deployment, fully controllable mobility and low cost. In fact, with the assistance of UAVs, the system performance (e.g., data rate and latency)

can be significantly enhanced by establishing the line-of-sight (LoS) communication links between UAVs and user equipments (UEs). In addition, through dynamically adjusting the flying state, UAVs are capable of improving communication performance in wireless communications. To further improve the channel quality, adaptive communications can be designed through the mobility control of the UAV systems.

In order to fully exploit the potential of UAV-assisted communications, it is crucial to design appropriate path planning and trajectory of UAVs [1]. In [2], Hourani *et al.* proposed an analytical approach for optimizing the altitude of UAV for the purpose of maximizing the radio coverage on the ground. In [3], a practical scenario of UAVs in an OFDMA system was investigated, and Wu *et al.* proposed an iterative block coordinate descent approach for optimizing the UAV's trajectory and OFDMA resource allocation, aiming to maximize the minimum average throughput of UEs. The optimization problem of UAV placement and transmit power in UAV-aided relay systems was studied in [4], where Ren *et al.* proposed a low-complexity iterative algorithm to solve the problem both in the free-space channel and three-dimensional channel scenarios. In [5], to minimize the energy consumption of UAV, Zeng *et al.* formulated a travelling sale problem and proposed an efficient algorithm to optimize the UAV trajectory, including the hovering locations and duration. Another category of UAV-assisted communication that considers a fixed-wing UAV was studied in [6], where the UAV usually applies higher speed and heavier payload and fly in the forward motion. The authors of [6] optimized the speed, direction, and acceleration of the UAV for maximizing the energy efficiency. In [7], a multi UAV-assisted communication system was studied. The authors proposed a *DRL-EC*<sup>3</sup> algorithm to optimize the UAVs' trajectory for maximizing the energy efficiency of UAVs. Other contributions of UAV include its applications in mobile edge computing (MEC) [8], device-to-device communication [9], data collection [10], mobile crowd sensing [11] and wireless power transfer networks [12]. In [8], Yang *et al.* studied the power minimization problem in a multi UAV-enabled MEC system, where they proposed a low complexity algorithm for optimizing the user association, power control, computation capacity allocation and location planning. In [9], Huang *et al.* investigated the D2D rate maximization problem in UAV-aided wireless communication systems, where they proposed an iterative algorithm for optimizing the UAV flying altitude,

Liang Wang, Kezhi Wang and Nauman Aslam are with the Department of Computer and Information Science, Northumbria University, Newcastle upon Tyne, NE1 8ST, U.K., emails: {liang.wang, kezhi.wang, nauman.aslam}@northumbria.ac.uk.

Cunhua Pan is with School of Electronic Engineering and Computer Science, Queen Mary University of London, E1 4NS, U.K., email: c.pan@qmul.ac.uk.

Wei Xu is with National Mobile Communications Research Lab, Southeast University, 210096, China, email: wxu@seu.edu.cn.

location and the bandwidth allocation, which proved that the altitude of the UAV is vital for improving the system performance. In [10], the UAV system was deployed as a mobile data collector in wireless sensor network, and the authors optimized the sensor nodes' wake up schedule and UAV trajectory for minimizing the maximum energy consumption of all sensor nodes. In [11], Liu *et al.* introduced a distributed mobile crowd sensing platform, where multiple UAVs are deployed as mobile terminals for collecting data. They proposed a DRL-based approach for navigating a group of UAVs in order to maximize the collected data, the geographical fairness, and the energy efficiency of UAVs. In [12], Xu *et al.* studied the problem of maximizing the energy harvested at all energy receivers in a UAV-enabled wireless power transfer system, in which they first proposed an algorithm based on Lagrange dual method for optimizing UAV trajectory in an ideal case. Then, they also proposed a new successive hover-and-fly algorithm based on convex programming optimization for trajectory design for the general case.

However, in the crowded area, the communication signals between UAV and UE may be blocked by high buildings or other constructions. Recently, thanks to the development of meta-materials [13], intelligent reflecting surface (IRS) [14] has been proposed and received considerable attention in both academia and industry, which has the potential to improve the communication quality by installing IRSs on the wall of the buildings. In general, the IRS consists of an array of low-cost and passive reflecting elements, each of which is able to reflect the incident signals by smartly adjusting the phase shift, which has the potential to improve the achievable data rate significantly [15]. Furthermore, since the reflecting elements of the IRS are usually passive and thus reflect signals without any signal processing tasks, the IRS is more energy-efficient than traditional relay-aided communication techniques, such as [16]. In addition, as the reflecting elements of IRS are reconfigurable in real time, the IRS can be viewed as a feasible transmission medium and widely deployed in the buildings and walls.

Due to the above advantages, the IRS was extensively investigated in various wireless communication systems. In [17], an IRS-enhanced MISO wireless system was studied, and the authors proposed a semidefinite relaxation (SDR) based algorithm for optimizing the active and passive beamforming, aiming to maximize the overall received signal power at the user. In [18], Yang *et al.* studied a realistic IRS-enhanced OFDM system, where the frequency-selective channels were considered, and the passive array reflecting coefficients were optimized for maximizing the achievable rate of the user. For multi-user communication systems, Huang *et al.* [19] investigated the energy efficiency maximization problem, and they proposed a sequential fractional programming based algorithm for optimizing the IRS phase shifts, which has 300% higher energy efficiency compared with the existing benchmarks. In order to enhance the physical layer security of IRS-aided communication systems, Yu *et al.* [20] jointly optimized the beamforming at the transmitter and the phase shifts of the IRS, maximizing the physical layer security data rate. For multicast scenarios, the authors in [21] investigated the downlink IRS-

aided multigroup multicast communication system, where the IRS can be deployed to enhance the worst-case user channel condition. In [22], Pan *et al.* studied the weighted sum rate (WSR) maximization problem for an IRS-assisted multicell MIMO communication system, and the authors proposed a pair of algorithms named Majorization-Minimization (MM) and Complex Circle Manifold (CCM) for optimizing the phase shifts of the IRS. The simulation results in [22] shows that the IRS is very effective in mitigating the cell-edge interference. Additionally, the authors in [23] considered to deploy an IRS in a simultaneous wireless information and power transfer (SWIPT) system to enhance both the energy harvesting and data rate performance. In [24], the IRS was shown to be beneficial in reducing the latency of the mobile edge computing system.

In [25], the authors studied the resource allocation for a point-to-point IRS-aided MIMO communication system when taking into account the channel estimation and channel feedback overhead. In [26], the globally optimal active and passive beamforming is obtained through the branch-and-bound algorithm for a single-user IRS-aided MISO system. In [27], the deep reinforcement learning was adopted to solve the joint transmit beamforming matrix at the base station and the phase shift matrix at the RIS.

Most recently, the integration of IRS in UAV-assisted communication systems is becoming a hot research topic, and the key challenge is to tackle the joint UAV trajectory and passive beamforming optimization problem. In [28], the authors considered a downlink transmission system, consisting of a rotary-wing UAV, a ground user and an IRS. In this work, the authors proposed a successive convex approximation (SCA) based algorithm to optimize the UAV trajectory and passive beamforming of the IRS. In [29], the potential of IRS in UAV-assisted communication systems was investigated. The authors concluded that the deployment of IRS is capable of achieving significant performance gain in UAV-assisted cellular networks. However, most of existing algorithms are based on convex optimization theory, which could only achieve sub-optimal or near-optimal performance and is time-consuming due to the fact that a number of iterations are required for the convergence of the algorithm. Their complexity increases drastically with the number of reflecting elements, UAVs and IRSs.

Thanks to the advances in the field of machine learning, most of sophisticated optimization problems can be solved efficiently and can be deployed in real time. As a branch of machine learning algorithm, reinforcement learning (RL) is viewed as a useful approach for tackling complicated control tasks, such as robotics and games. In [30], Sutton *et al.* proposed a widely used model-free RL algorithm named Q-learning, where some fundamental knowledge, such as agent, environment, state, action, reward and Q-value were introduced. In addition, another mechanism named Q-table was employed in Q-learning. However, as the size of Q-table is finite, Q-learning can only handle control problems in discrete state and action spaces. As an extension of Q-learning, Mnih *et al.* [31] proposed the deep Q-network (DQN) algorithm, which combines RL and the powerful deep neural network (DNN).

Additionally, two techniques named experience replay and target network were integrated. The experimental results proved that DQN is capable of achieving enhanced performance in the challenging Atari 2600 games. In DQN, the Q-table is replaced by the DNN, as DQN can handle the control problem with infinite state spaces. However, the action space of DQN is still discrete. Inspired by DQN, Silver *et al.* proposed a deep deterministic policy gradient (DDPG) [32] algorithm based on the actor-critic [33] method, which is able to be applied to continuous action spaces.

Against the above background, we propose an IRS-aided UAV system where the UAV is deployed to provide communication services to the ground UEs. To enhance the channel condition between UAV and UEs, which may be blocked by some obstacles such as high buildings, IRS is proposed to be mounted on the exterior wall of the buildings. We aim to maximize the overall weighted data rate and geographical fairness of all the UEs via jointly optimizing the UAV's trajectory and the phase shifts of the reflecting elements of IRSs. To address this problem, firstly, we propose a deep Q-network (DQN)-based low-complex solution by discretizing the trajectory and phase shift, which can be useful for practical systems with discrete phase-shift control. Then, we further propose a deep deterministic policy gradient (DDPG)-based solution to tackle the continuous counterpart. The experiment verifies that the proposed algorithms achieve better performance compared to other traditional benchmarks.

The remainder of this paper is organized as follows. In Section II, we describe the system model, including the optimization problem. In Section III, we present the proposed DQN and DDPG algorithms. In Section IV, the experimental results are analyzed. Finally, we conclude the paper in Section V. In addition, the main notations used in this paper are summarized in Table. I.

*Other Notations:* In this paper,  $\mathbb{C}^{M \times 1}$  denotes the set of  $M \times 1$  complex vectors.  $\text{diag}\{\cdot\}$  denotes the diagonalization operation.  $(\cdot)^H$  denotes the conjugate transpose operation.  $\mathbb{E}[\cdot]$  denotes the expectation operation.  $|\cdot|$  denotes the determinant operation.

## II. SYSTEM MODEL

Assume that there is one rotary UAV,  $K$  IRSs mounted on  $K$  buildings respectively and  $N$  UEs to be served, as shown in Fig. 1. We assume that the UAV serves all the UEs via the downlink transmission system. Also, assume that the UEs are located in the crowded area where they suffer from severe path loss and high attenuation, caused by tall buildings and trees. IRSs are deployed for enhancing the communication quality of UEs. As shown in Fig.1, the UAV flies at a fixed altitude  $H^U$  (in meters) over a rectangle target area with side lengths  $[X^{max}, Y^{max}]$  for a certain period of time  $T^{all}$ . We denote the set of IRSs as  $\mathcal{K} \triangleq \{k = 1, 2, \dots, K\}$  and the set of UEs as  $\mathcal{N} \triangleq \{n = 1, 2, \dots, N\}$ . For simplicity, we divide  $T^{all}$  into  $T$  time slots (TSS), each of which has the maximal time duration  $T^d$ . Also, the set of TSSs is denoted as  $\mathcal{T} \triangleq \{1, 2, \dots, T\}$ . Additionally, each IRS is equipped with a uniform linear array (ULA) with  $M$  reflecting elements, which could

TABLE I: Main Notations.

Notation	Definition
$k, K, \mathcal{K}$	the index, the number, and the set of IRSs
$n, N, \mathcal{N}$	the index, the number, and the set of UEs
$t, T, \mathcal{T}$	the index, the number, and the set of TSSs
$m_k, \mathcal{M}_k$	the index, the set of reflecting elements of IRS $k$
$M$	the number reflecting elements of each IRS
$\mu_t, d_t$	flying angle, distance of UAV in TS $t$
$[X_0^U, Y_0^U, H^U]$	coordinates of UAV in the initial TS
$[X_t^U, Y_t^U, H^U]$	coordinates of UAV in TS $t$
$X^{max}, Y^{max}$	side length of the target area
$v_t$	velocity of UAV in TS $t$
$T^d$	time duration of each TS
$d^{max}$	maximal flying distance of UAV in each TS
$U_r$	tip speed of the rotor blade
$V_h$	mean rotor induced velocity when hovering
$d_0$	main body drag ratio
$\rho_a$	air density
$z$	rotor solidity
$A$	the rotor disc area
$e_t$	remaining energy level of UAV in TS $t$
$e^{max}$	maximal energy level of UAV
$[X_k^I, Y_k^I, H_k^I]$	coordinates of IRS $k$
$[x_n, y_n]$	coordinates of UE $n$
$d_{k,t}^{UI}$	distance between UAV and IRS $k$ in TS $t$
$d_{n,k}^{IE}$	distance between IRS $k$ and UE $n$
$h_{k,t}^{UI}$	channel gain between UAV and IRS $k$ in TS $t$
$h^{UI}$	overall channel gain between UAV and IRSs in TS $t$
$h_{n,k}^{IE}$	channel gain between IRS $k$ and UE $n$ in TS $t$
$h_n^{IE}$	overall channel gain between IRSs and UE $n$
$R_{n,t}$	data rate of UE $n$ to in TS $t$
$\sigma^2$	noise variance
$P$	transmit power of UAV
$c_{n,t}$	serving status of UE $n$ in TS $t$
$k_i, k_q$	weight factors
$\gamma$	discount factor
$s_t, a_t, r_t$	state, action, reward in TS $t$
$p$	penalty

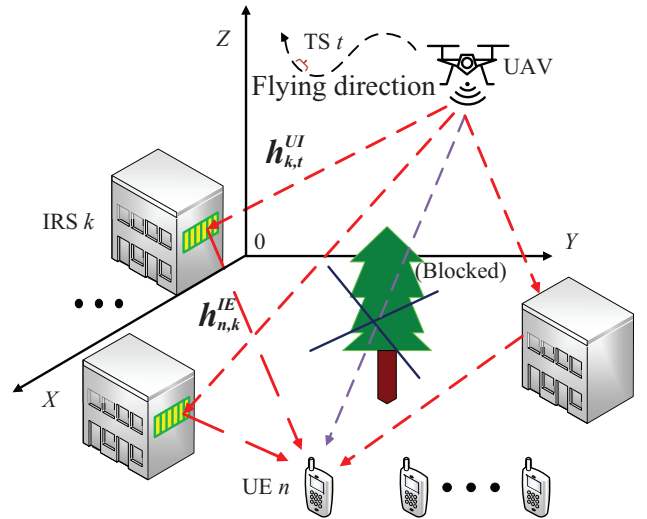


Fig. 1: Architecture of IRS-assisted UAV communication system

boost the useful signal power by adjusting the phase shifts of the reflecting elements. As a result, the set of reflecting elements of IRS  $k$  is denoted as  $\mathcal{M}_k \triangleq \{1, 2, \dots, M\}$ . Also, assume that all the IRSs are in parallel with the XOZ plane, similar to [28], shown in Fig. 1.

#### A. UAV model

In each TS, the UAV will move with a flying action determined by the angle of  $\mu_t \in [0, 2\pi)$  and a distance of  $d_t \in [0, d^{max}]$ . It is assumed that the initial coordinate of the UAV is  $[X_0^U, Y_0^U, H^U]$ . Thus, the coordinate of UAV in TS  $t$  is denoted by  $[X_t^U, Y_t^U, H^U]$ , where

$$X_t^U = X_0^U + \sum_{t'=1}^t d_{t'} \cos \mu_{t'}, \quad \forall t \in \mathcal{T}, \quad (1)$$

and

$$Y_t^U = Y_0^U + \sum_{t'=1}^t d_{t'} \sin \mu_{t'}, \quad \forall t \in \mathcal{T}. \quad (2)$$

It is worth mentioning that the UAV cannot go beyond the border of the targeted area, which can be represented as

$$0 \leq X_t^U \leq X^{max}, \quad \forall t \in \mathcal{T}, \quad (3)$$

and

$$0 \leq Y_t^U \leq Y^{max}, \quad \forall t \in \mathcal{T}. \quad (4)$$

In each TS, the UAV flies with a constant velocity  $v_t$ , which can be denoted by

$$v_t = \frac{d_t}{T_d}, \quad \forall t \in \mathcal{T}. \quad (5)$$

In this paper, the communication related energy, including communication circuitry and signal processing, is ignored compared with the propulsion energy. According to [5], the propulsion energy consumption in TS  $t$  with the velocity  $v_t$  can be expressed as

$$\begin{aligned} e_t^m = & \left( P_s \left( 1 + 3 \left( \frac{v_t}{U_r} \right)^2 \right) \right. \\ & + P_m \left( \sqrt{1 + \frac{1}{4} \left( \frac{v_t}{V_h} \right)^4} - \frac{1}{2} \left( \frac{v_t}{V_h} \right)^2 \right)^{\frac{1}{2}} \\ & \left. + \frac{1}{2} d_0 \rho_a z A v_t^3 \right) T^d, \quad \forall t \in \mathcal{T}, \end{aligned} \quad (6)$$

where  $P_s$  and  $P_m$  are fixed constants and can be obtained from [5];  $U_r$  is the tip speed of the rotor blade;  $V_h$  denotes the mean rotor induced velocity when hovering;  $d_0$  is the main body drag ratio;  $\rho_a$  is the air density;  $z$  means the rotor solidity; and  $A$  is known as the rotor disc area. The remaining energy level  $e_t$  of UAV in TS  $t$  is given by

$$e_t = e^{max} - \sum_{t'=1}^t e_{t'}^m, \quad (7)$$

where  $e^{max}$  is the maximal energy level that UAV possess except the necessary energy for taking off and landing. Additionally, we assume the process that the UAV serves UEs is terminated until the remaining energy of UAV is consumed. Thus, we can have

$$0 \leq e_t, \quad \forall t \in \mathcal{T}. \quad (8)$$

#### B. Channel model

In this paper, as shown in Fig. 1, due to the obstacles, such as trees and tall buildings, we assume that the direct link between the UAV and the UEs are blocked. To resolve this issue, the IRSs are installed at the walls of other buildings to reflect the signals from the UAV to the UEs. Denote the coordinate of IRS  $k$  as  $[X_k^I, Y_k^I, H_k^I]$ , the coordinate of UE  $n$  as  $[x_n, y_n]$ . Thus, the distance between UAV and IRS  $k$  in TS  $t$  is expressed as

$$d_{k,t}^{UI} = \sqrt{(X_t^U - X_k^I)^2 + (Y_t^U - Y_k^I)^2 + (H^U - H_k^I)^2}. \quad (9)$$

Similarly, the distance between IRS  $k$  and UE  $n$  is given by

$$d_{n,k}^{IE} = \sqrt{(X_k^I - x_n)^2 + (Y_k^I - y_n)^2 + (H_k^I)^2}. \quad (10)$$

In this paper, we assume that the signal transmission operates in mmWave communications, where line-of-sight (LoS) communication is ensured for both the UAV-IRS and IRS-UE links. As a results, the channel gain of the UAV-IRS  $k$  link in TS  $t$  is denoted by  $\mathbf{h}_{k,t}^{UI} \in \mathbb{C}^{M \times 1}$ , which can be expressed as

$$\mathbf{h}_{k,t}^{UI} = \sqrt{\frac{\alpha}{(d_{k,t}^{UI})^2}} \left[ 1, e^{-j \frac{2\pi}{\lambda} d \phi_{k,t}^{UI}}, \dots, e^{-j \frac{2\pi}{\lambda} (M-1) d \phi_{k,t}^{UI}} \right]^T, \quad (11)$$

where  $\alpha$  is the path loss at the reference distance of 1 meter, the right term in Eq. (11) means the array response of IRS  $k$  with  $M$  reflecting elements in TS  $t$  [34], where  $\phi_{k,t}^{UI} = \frac{X_k^I - X_t^U}{d_{k,t}^{UI}}$  can approximately represent the cosine value of the angle of arrival (AoA) of the UAV-IRS  $k$  link in TS  $t$ .  $\lambda$  is the carrier wavelength, and  $d$  is the antenna separation distance.

Thus, the overall channel gain of UAV-IRS links in TS  $t$ , denoted by  $\mathbf{h}_t^{UI} \in \mathbb{C}^{MK \times 1}$ , can be given by

$$\mathbf{h}_t^{UI} = \left[ \mathbf{h}_{1,t}^{UI}, \mathbf{h}_{2,t}^{UI}, \dots, \mathbf{h}_{K,t}^{UI} \right]^T. \quad (12)$$

Similarly, the channel gain of the IRS  $k$ -UE  $n$  link, denoted by  $\mathbf{h}_{n,k}^{IE}$ , is expressed as

$$\mathbf{h}_{n,k}^{IE} = \sqrt{\frac{\alpha}{(d_{n,k}^{IE})^\beta}} \left[ 1, e^{-j \frac{2\pi}{\lambda} d \phi_{n,k}^{IE}}, \dots, e^{-j \frac{2\pi}{\lambda} (M-1) d \phi_{n,k}^{IE}} \right]^T, \quad (13)$$

where  $\beta$  denotes the path loss exponent, which is related to the IRS-UE link, and  $\phi_{n,k}^{IE} = \frac{X_k^I - x_n}{d_{n,k}^{IE}}$  approximately represents the cosine value of the angle of departure (AoD) of the IRS  $k$ -UE  $n$  link. Then, the overall channel gain  $\mathbf{h}_n^{IE} \in \mathbb{C}^{MK \times 1}$  of IRS-UE  $n$  is expressed as

$$\mathbf{h}_n^{IE} = \left[ \mathbf{h}_{n,1}^{IE}, \mathbf{h}_{n,2}^{IE}, \dots, \mathbf{h}_{n,K}^{IE} \right]^T. \quad (14)$$

In this paper, we assume that the UAV can only serve one UE in each TS. We define  $c_{n,t}$  as the serving status of UE  $n$  in TS  $t$ , which is given by

$$c_{n,t} = \{0, 1\}, \quad \forall n \in \mathcal{N}, t \in \mathcal{T}, \quad (15)$$

where  $c_{n,t} = 1$  means that the UAV sends data to UE  $n$  in TS  $t$ , otherwise  $c_{n,t} = 0$ . Thus, we have

$$\sum_{n=1}^N c_{n,t} = 1, \quad \forall t \in \mathcal{T}. \quad (16)$$

Assume that the UAV always communicates to the UE which has the maximal data rate in each TS. Then, one has

$$c_{n,t} = \begin{cases} 1, & n = \operatorname{argmax}_{n' \in \mathcal{N}} (R_{n',t}), \\ 0, & \text{otherwise.} \end{cases} \quad (17)$$

Additionally, motivated by [35], we introduce the Jain's fairness index  $f_t$  as follows

$$f_t = \frac{(\sum_{n=1}^N \sum_{t'=1}^t c_{n,t'})^2}{N \sum_{n=1}^N (\sum_{t'=1}^t c_{n,t'})^2}, \quad (18)$$

where  $f_t \in [0, 1]$  represents the level of fairness from the initial TS up to TS  $t$ . In particular, if all UEs are served for approximately equal number of TSs,  $f_t$  is closer to 1, and otherwise  $f_t$  is closer to 0.

We denote  $\theta_{k,n,m,t} \in [0, 2\pi)$  as the diagonal phase shift of the reflecting element  $m$  of IRS  $k$  to UE  $n$  in TS  $t$ . Thus, the overall diagonal phase shift matrix for IRSs to UE  $n$  in TS  $t$  is  $\Theta_{n,t} = \operatorname{diag}\{e^{j\theta_{k,n,m,t}}, \forall m \in \mathcal{M}, k \in \mathcal{K}\}$ .

According to Eq.(12) and (14), the achievable data rate of the UE  $n$  in TS  $t$  is given by

$$R_{n,t} = \log_2 \left( 1 + \frac{P |(\mathbf{h}_n^{IE})^H \Theta_{n,t} \mathbf{h}_t^{UI}|^2}{\sigma^2} \right), \quad (19)$$

where  $P$  is the transmit power of the UAV, and  $\sigma^2$  is the noise power.

### C. Problem Formulation

We aim to maximize the weighted fairness and data rate for all the users, which can be formulated as the following optimization problem

$$\max_{\Theta, \mathbf{Z}, \mathbf{T}} \sum_{t=1}^T (k_i \cdot f_t + k_q \cdot \sum_{n=1}^N c_{n,t} R_{n,t}) \quad (20a)$$

subject to:

$$0 \leq X_t^U \leq X^{max}, \quad \forall t \in \mathcal{T}, \quad (20b)$$

$$0 \leq Y_t^U \leq Y^{max}, \quad \forall t \in \mathcal{T}, \quad (20c)$$

$$0 \leq e_t, \quad \forall t \in \mathcal{T}, \quad (20d)$$

$$0 \leq \mu_t < 2\pi, \quad \forall t \in \mathcal{T}, \quad (20e)$$

$$0 \leq d_t \leq d^{max}, \quad \forall t \in \mathcal{T}, \quad (20f)$$

$$0 \leq \theta_{k,n,m,t} < 2\pi, \quad \forall k \in \mathcal{K}, n \in \mathcal{N}, m \in \mathcal{M}, t \in \mathcal{T}, \quad (20g)$$

$$c_{n,t} \in \{0, 1\}, \quad \forall n \in \mathcal{N}, t \in \mathcal{T}, \quad (20h)$$

$$\sum_{n=1}^N c_{n,t} = 1, \quad \forall t \in \mathcal{T}, \quad (20i)$$

where  $\Theta = \{\Theta_{n,t}, \forall n \in \mathcal{N}, t \in \mathcal{T}\}$ ,  $\mathbf{Z} = \{X_t^U, Y_t^U, \forall t \in \mathcal{T}\}$ ,  $\mathbf{T} = \{t, \forall t \in \mathcal{T}\}$ .  $k_i$  and  $k_q$  are weight factors. It is quite difficult to solve the above problem in general since it involves a mixture of continuous and integer variables. We first

propose a DQN-based algorithm to solve the above problem by discretizing the variables  $\Theta$  and  $\mathbf{Z}$  first. This can reduce the complexity of the algorithm, although it may result in a little bit of performance loss. Additionally, this DQN-based solution is useful in the scenario where the hardware has some limitations, i.e., the phase may only be adjusted discretely. Next, to tackle the variables with continuous scenarios, we further propose a DDPG-based algorithm to address it. This applies to the system where the phase shifts of IRS can be adjusted continuously.

### III. DQN-BASED SOLUTION FOR DISCRETE CASES

In this section, we propose the DQN-based algorithm. We first introduce the state, action and reward. Then, we model the whole IRS-assisted UAV communication system as an environment. It is assumed that the agent is employed for interacting with the environment with the objective of finding the optimal actions that can maximize the accumulated rewards  $R_t = \sum_{t'=t}^T \gamma^{t'-t} r_{t'}$  within a sequence of states, where  $\gamma \in [0, 1]$  is the discount factor. In this paper, we define the state  $s_t$ , the action  $a_t$ , and the reward  $r_t$  in TS  $t$  as follows:

- 1) State  $s_t$ : the state of agent in TS  $t$  has two components.
  - a) UAV's current coordinate:  $\{X_t^U, Y_t^U\}$ .
  - b) UAV's current energy level:  $\{e_t\}$ .
- 2) Action  $a_t$ : we define the UAV's flying direction  $\mu_t$ , distance  $d_t$  in TS  $t$  as action  $a_t = \{\mu_t, d_t\}$ . The relations between the coordinates of the UAV and the actions can be found in (1) and (2).
- 3) Reward  $r_t$ : we define the reward function as:

$$r_t = f_t + \frac{k_q}{k_i} \cdot \sum_{n=1}^N c_{n,t} R_{n,t} - p, \quad (21)$$

where  $p$  is defined as the penalty if the UAV flies out of the target area.

Motivated by the work that is done in [31], here we propose the DQN-based algorithm for optimizing the UAV trajectory. Additionally, we assume that the phase shifts are discretized, which is useful in practical finite phase-shift control due to hardware limit. We show the process of optimizing the UAV trajectory by introducing the architecture of the DQN algorithm. As shown in Fig. 2, there is an agent which controls the UAV for interacting with the environment. We assume there are two DQNs named the evaluation network and target network. Note that the target network has the same structure with the evaluation network but it only updates periodically. Firstly, the agent sends the state  $s_t$  to the evaluation network, which generates the Q-values  $Q(s_t, a_t)$  of all actions. Based on the Q-values and following an  $\epsilon$ -greedy policy, the action  $a_t$  is generated. After that, the reward  $r_t$  is obtained from the environment. It is worth mentioning that the proposed DQN-based algorithm can only optimize the UAV trajectory in the finitely discrete action space. Hence, the flying angle is assumed to be chosen from the following finite values:

$$\mu_t \in \left\{ \frac{2\pi}{N^\mu} i, i = 0, 1, \dots, N^\mu - 1 \right\}, \quad (22)$$

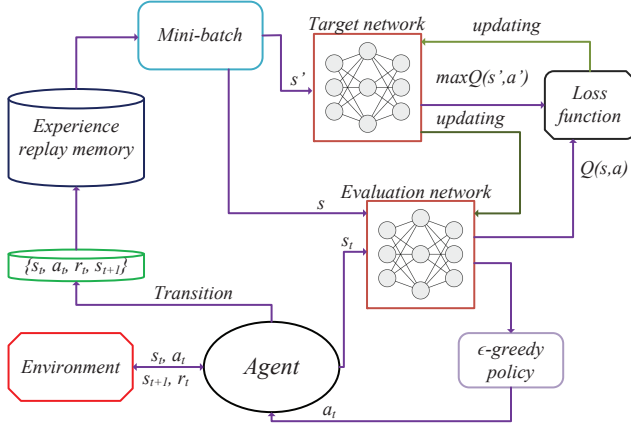


Fig. 2: Structure of DQN algorithm

where  $N^\mu$  is the number of flying directions we can select. Also, the flying distance is chosen from the following finite values:

$$d_t \in \left\{ \frac{d^{max}}{N^d} l, l = 1, \dots, N^d \right\}, \quad (23)$$

where  $N^d$  is the number of flying distances we can choose. Hence, the action set of the UAV can be denoted as  $\mathcal{A} \triangleq \left\{ \left[ \frac{2\pi}{N^\mu} i, \frac{d^{max}}{N^d} l \right], i = 0, 1, \dots, N^\mu - 1, l = 1, \dots, N^d \right\}$ .

Then, the transition, which consists of  $[s_t, a_t, r_t, s_{t+1}]$  is stored into an experience replay memory. When the experience replay memory with the size of  $m^{max}$  has enough transitions, the learning procedure starts. A mini-batch randomly samples  $K$  transitions to train the DQNs. Precisely, given the Q-values  $Q(s, a)$  from the evaluation network and the maximal Q-values  $\max Q(s', a')$  from the target network, the loss function can be calculated for updating the evaluation network, which can be expressed as

$$L_i(\delta_i) = \mathbb{E}_{s,a} \left[ \left( r + \gamma \max_{a'} Q(s', a') | \delta_{i-1} - Q(s, a | \delta_i) \right)^2 \right], \quad (24)$$

where  $\delta$  is the parameter of the DQN, and  $i$  is the index of iteration.

Then, we introduce the quantitative passive beamforming approach for optimizing the phase shifts of IRSs. Precisely, Eq. (11) can be also transformed into the following equation

$$\mathbf{h}_{k,t}^{UI} = \left[ |\mathbf{h}_{k,t}^{UI}| e^{j\omega_{k,1,t}^{UI}}, |\mathbf{h}_{k,t}^{UI}| e^{j\omega_{k,2,t}^{UI}}, \dots, |\mathbf{h}_{k,t}^{UI}| e^{j\omega_{k,M,t}^{UI}} \right]^T, \quad (25)$$

where  $|\mathbf{h}_{k,t}^{UI}|$  is the magnitude and  $\omega_{k,m,t}^{UI} \in [0, 2\pi)$  is the phase shift of the reflecting element  $m$  of IRS  $k$  in TS  $t$ . Similarly, we transfer Eq. (13) into the following

$$\mathbf{h}_{n,k}^{IE} = \left[ |\mathbf{h}_{n,k}^{IE}| e^{j\omega_{n,k,1}^{IE}}, |\mathbf{h}_{n,k}^{IE}| e^{j\omega_{n,k,2}^{IE}}, \dots, |\mathbf{h}_{n,k}^{IE}| e^{j\omega_{n,k,M}^{IE}} \right]^T, \quad (26)$$

where  $|\mathbf{h}_{n,k}^{IE}|$  denotes the magnitude and  $\omega_{n,k,m}^{IE} \in [0, 2\pi)$  is the phase shift of reflecting element  $m$  of IRS  $k$  to UE  $n$ .

For simplicity, we consider a discrete version of constraint (20g). In particular, the phase shift of the IRS is chosen from

the following set of  $\Upsilon \triangleq \left\{ \frac{2\pi}{N^I} i, i = 0, 1, \dots, N^I - 1 \right\}$ , where  $N^I$  is the number of phase shift values that each element can select. This also means the IRS can only reflect the signals with some specific phase shifts due to the hardware limits.

Also, one can see that if the signals from different paths are combined coherently at the UE, the maximal received signal power can be achieved, which will theoretically maximize the achievable data rate. Thus, we optimize the phase shift  $\theta_{k,n,m,t}$  of reflecting element  $m$  of IRS  $k$  to UE  $n$  in TS  $t$  with the following equation

$$\theta_{k,n,m,t} = \underset{\theta'_{k,n,m,t} \in \Upsilon}{\operatorname{argmin}} \left| \theta'_{k,n,m,t} - (\omega_{k,m,t}^{UI} + \omega_{n,k,m}^{IE}) \right|. \quad (27)$$

One can see that we only can select limited number of reflecting phases.

In Algorithm 1, we provide the overall pseudo code of the proposed algorithm. From Line 1 to 3, we initialize the

---

#### Algorithm 1 DQN-based algorithm

---

- 1: Initialize evaluation network with parameters  $\delta$ ;
  - 2: Initialize target network with parameters  $\delta$ ;
  - 3: Initialize experience replay memory with size  $m^{max}$ ;
  - 4: **for** Episode = 1,2,..., $N^{eps}$  **do**
  - 5:    $t = 0$ ;
  - 6:   Initialize state  $s_t = [X_0^U, Y_0^U, e^{max}]$ ;
  - 7:   Initialize vector  $\mathbf{F}$  with size  $N$ ;
  - 8:   **while**  $e_t > 0$  **do**
  - 9:     Obtain  $s_t$ ;
  - 10:     Select  $a_t = \underset{a_t \in \mathcal{A}}{\operatorname{argmax}} Q(s_t, a_t)$  with probability  $\epsilon$ ;
  - 11:     Randomly select  $a_t$  from  $\mathcal{A}$  with probability  $1 - \epsilon$ ;
  - 12:     Execute  $a_t$ ;
  - 13:     Obtain  $e_t$  from Eq. (7);
  - 14:     Initialize vector  $\mathbf{R}$  with size  $N$ ;
  - 15:     **for** UE  $n = 1, 2, \dots, N$  **do**
  - 16:       Obtain the optimized phase shift of each element of IRSs in TS  $t$  from Eq. (27);
  - 17:       Calculate the data rate  $R_{n,t}$  of UE  $n$  according to Eq. (19);
  - 18:        $\mathbf{R}(n) \leftarrow R_{n,t}$ ;
  - 19:     **end for**
  - 20:      $n = \underset{n \in \mathcal{N}}{\operatorname{argmax}} \mathbf{R}$ ;
  - 21:      $\mathbf{F}(n) \leftarrow \mathbf{F}(n) + 1$ ;
  - 22:     Calculate  $f_t$  from  $\mathbf{F}$ ;
  - 23:     Obtain  $r_t$  according to Eq. (21);
  - 24:     Store transition  $[s_t, a_t, r_t, s_{t+1}]$  into experience replay memory;
  - 25:     **if** the learning process starts **then**
  - 26:       Randomly sample  $K$  transitions from experience replay memory;
  - 27:       Update evaluation network from Eq. (24);
  - 28:       Update target network periodically;
  - 29:     **end if**
  - 30:      $t = t + 1$ ;
  - 31:   **end while**
  - 32: **end for**
- 

evaluation and target networks as well as the experience replay

memory. Then, during each episode, we first initialize the state  $s_t$  and the vector of  $\mathbf{F}$  with size  $N$  which is used for recording the times of each UE served from the initial TS up to TS  $t$ . Note that  $\mathbf{F}$  is applied to calculate  $f_t$ . Then, in each TS, the agent follows an  $\epsilon$ -greedy policy to generate  $a_t$ . Precisely, the agent selects  $a_t$  that has the maximal Q-value with probability  $\epsilon$ , or randomly selects  $a_t$  from  $\mathcal{A}$  with probability  $1-\epsilon$ . In Line 14, we initialize the vector  $\mathbf{R}$  to record the data rate  $R_{n,t}$  of each UE in TS  $t$ . From Line 15 to 18, the optimized phase shift of each element of IRSs is calculated according to Eq. (27). The data rate of each UE in TS  $t$  is calculated from Eq. (19). Then, given  $\mathbf{R}$ , the UE that has the maximal data rate is selected to be served by the UAV. Additionally,  $r_t$  is calculated by Eq. (21). After that, the transition  $[s_t, a_t, r_t, s_{t+1}]$  is stored into the experience replay memory. When the learning process starts,  $K$  transitions are randomly sampled for training the evaluation network by Eq. (24). Then, the target network is updated periodically.

#### IV. DDPG-BASED SOLUTION FOR CONTINUOUS CASES

In this subsection, we propose the DDPG-based algorithm for tackling the continuous case and optimizing the UAV trajectory and passive beamforming of IRSs. The UAV trajectory optimization problem is firstly tackled by the DDPG-based algorithm, which applies the well-known actor-critic approach. We also show the architecture of DDPG algorithm in Fig. 3. There are two DQNs named actor network with function

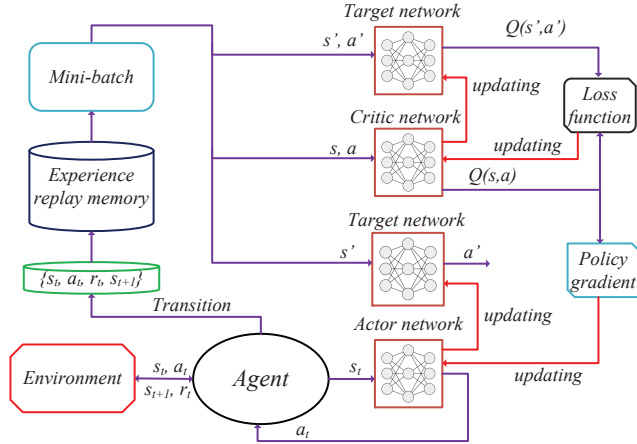


Fig. 3: Structure of DDPG algorithm

$a = \pi(s|\delta^\pi)$  and critic network with function  $Q(s, a|\delta^Q)$  respectively. Note that  $\pi(\cdot)$  maps the state and action,  $Q(\cdot)$  is the approximator for generating Q-value with the given state-action pairs. Also, there are two target networks with function  $\pi'(\cdot)$  and  $Q'(\cdot)$ , which have the same structure with actor and critic networks, respectively. The agent sends the state  $s_t$  and directly receives the action  $a_t$  generated by the actor network. It is worth mentioning that the flying direction and distance of UAV in TS  $t$  can be expressed respectively as follows

$$\mu_t = x_t^\mu \pi, \quad (28)$$

and

$$d_t = |x_t^d| d_{max}, \quad (29)$$

where  $x_t^\mu$  and  $x_t^d$  are the output of actor network. Note that in this paper, we denote  $\tanh(\cdot)$  as the activation function of the output layer, which has  $x_t^\mu \in [-1.1]$ ,  $x_t^d \in [-1, 1]$ .

Then, the transition is stored into the experience replay memory with size of  $m^{max}$ . When the learning process starts, a mini-batch randomly samples  $K$  transitions to train the actor and critic networks. Precisely, given the state  $s$  and action  $a$ , the Q-value  $Q(s, a)$ , generated by the critic network, is used to calculate the policy gradient [32], which is expressed as

$$\nabla_{\delta^\pi} J = \mathbb{E} \left[ \nabla_a Q(s, a|\delta^Q) \Big|_{s=s_t, a=\pi(s_t|\delta^\pi)} \cdot \nabla_{\delta^\pi} \pi(s|\delta^\pi) \Big|_{s=s_t} \right]. \quad (30)$$

The actor network is trained according to the obtained policy gradient function. Then, the critic network is trained by the loss function [32] that is described as

$$L(\delta^Q) = \frac{1}{K} \sum_{k=1}^K (y_k - Q(s_k, \pi(s_k|\delta^\pi)|\delta^Q))^2, \quad (31)$$

where  $k$  is the index of transitions in mini-batch, and  $y_k = r_k + \gamma Q(s'_k, \pi'(s'_k|\delta^\pi)|\delta^Q)$ .

Based on the optimized UAV trajectory, we next optimize the phase shift of the reflecting elements of IRSs. Precisely, for any given UAV trajectory, the maximal data rate at UE is achieved if all the corresponding phases are aligned. Thus, we optimize the phase shift of element  $m$  of IRS  $k$  to UE  $n$  in TS  $t$  by the following equation [28]:

$$\theta_{k,n,m,t} = \omega_{k,m,t}^{UI} + \omega_{n,k,m}^{IE}. \quad (32)$$

Then, we provide the pseudo code of the proposed algorithm as shown in Algorithm 2. First of all, we initialize actor and critic networks with parameters  $\delta^\pi$  and  $\delta^Q$ , respectively. Besides, two target networks and the experience replay memory are initialized as well. During each training episode, we initialize the state  $s_t$  and a vector  $\mathbf{F}$  at the initial TS. The agent sends  $s_t$  and receives  $a_t$  generated by the actor network. Note that in Line 10,  $N'$  denotes the random noise,  $\eta$  decays with  $t$ , making the exploration successful. A vector  $\mathbf{R}$  with size  $N$  is employed for recording the data rate  $R_{n,t}$  of each UE in TS  $t$ . From Line 14 to 16, the phase shifts of each element of IRSs is obtained from Eq. (32). The data rate of each UE is calculated by Eq. (19). Then, based on  $\mathbf{R}$ , the UE that has the maximal data rate is served by the UAV. In Line 22, the reward  $r_t$  is calculated. After that, the transition  $[s_t, a_t, r_t, s_{t+1}]$  is stored into the experience replay memory. When the learning process starts, the mini-batch randomly samples  $K$  transitions to train the actor and critic network by Eq. (30) and Eq. (31). Additionally, two target networks are updated with the rate of  $\tau = 0.01$ .

#### V. SIMULATION RESULT

In this section, extensive simulations are conducted to evaluate the performance of the proposed solutions. The simulation is executed in Python 3.7 and Tensorflow 1.15.0. For DQN, we deploy three fully-connected hidden layers with [400, 300, 64]

**Algorithm 2** DDPG based algorithm

---

```

1: Initialize actor  $\pi(\cdot)$  and critic  $Q(\cdot)$  network with parameters  $\delta^\pi$  and  $\delta^Q$  respectively;
2: Initialize target networks  $\pi'(\cdot)$ ,  $Q'(\cdot)$  with parameters  $\delta^{\pi'} = \delta^\pi$ ,  $\delta^{Q'} = \delta^Q$ ;
3: Initialize experience replay memory with size  $m^{max}$ ;
4: for Episode = 1,2,..., $N^{eps}$  do
5:    $t = 0$ ;
6:   Initialize state  $s_t = [X_0^U, Y_0^U, e^{max}]$ ;
7:   Initialize vector  $\mathbf{F}$  with size  $N$ ;
8:   while  $e_t > 0$  do
9:     Obtain  $s_t$ ;
10:    Select  $a_t = \pi(s_t|\delta^\pi) + \eta N'$ ;
11:    Execute  $a_t$ ;
12:    Obtain  $e_t$  from Eq. (7);
13:    Initialize vector  $\mathbf{R}$  with size  $N$ ;
14:    for UE  $n = 1, 2, \dots, N$  do
15:      Obtain the optimized phase shift of each element of IRSs in TS  $t$  from Eq. (32);
16:      Calculate the data rate  $R_{n,t}$  of UE  $n$  according to Eq. (19);
17:       $\mathbf{R}(n) \leftarrow R_{n,t}$ ;
18:    end for
19:     $n = \operatorname{argmax} \mathbf{R}$ ;
20:     $\mathbf{F}(n) \leftarrow \mathbf{F}(n) + 1$ ;
21:    Calculate  $f_t$  from  $\mathbf{F}$ ;
22:    Obtain  $r_t$  according to Eq. (21);
23:    Store transition  $[s_t, a_t, r_t, s_{t+1}]$  into experience replay memory;
24:    if experience replay memory is full then
25:      Randomly sample  $K$  transitions from experience replay memory;
26:      Update critic network according to Eq. (31);
27:      Update actor network according to Eq. (30);
28:      Update two target networks with the rate of  $\tau$ ;
29:    end if
30:     $t = t + 1$ ;
31:  end while
32: end for

```

---

neurons and the AdamOptimizer is used to update DQNs with the rate of 0.00001. The number of flying directions of the UAV is set as  $N^\mu = 6$  and the number of flying distance values of UAV is set as  $N^d = 3$ . Also, the number of phase shift values of each reflecting element is set as  $N^l = 12$ . For DDPG-based solution, we deploy four fully-connected hidden layers with [400, 300, 256, 128] neurons in both actor and critic networks and AdamOptimizer is used to train the actor network with the rate of 0.0001 and critic network with the rate of 0.0002. The coordinates of IRSs are set as [100, 0, 100], [300, 0, 100], [500, 0, 100], [100, 200, 100], [300, 200, 100], [500, 200, 100], and the coordinates of UEs are set as [100, 50], [300, 50], [500, 50], [100, 150], [300, 150], [500, 150]. More parameters can be found in Table. II.

For comparison, we present two benchmark algorithms as follows:

TABLE II: Main Notations.

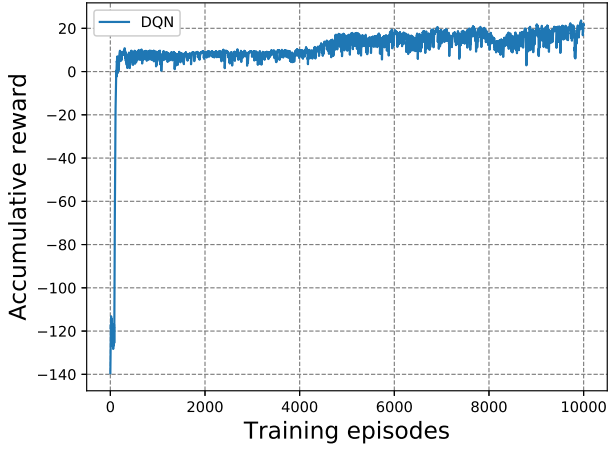
Notation	Description	Notation	Description
$K$	7	$N$	6
$M$	20	$X^{max}$	600 m
$Y^{max}$	200 m	$[X_0^U, Y_0^U, H^U]$	[10, 10, 200]
$T^d$	1 s	$T$	50
$d^{max}$	40 m	$\beta$	2.8
$\alpha$	-30 dB	$d$	$\frac{\lambda}{2}$
$U_r$	120 m/s	$V_h$	4.03
$d_0$	0.6	$\rho_a$	1.225 kg/m <sup>3</sup>
$z$	0.05	$A$	0.503 m <sup>2</sup>
$e^{max}$	20000	$P_s$	79.85
$P_m$	88.63	$\sigma^2$	-70 dBm
$P$	0.01 W	$k_i$	100
$k_q$	1	$N^\mu$	6
$N^d$	3	$N^l$	12
$N^{eps}$	10000	$\epsilon$	0.9
$N'$	1.3	$\gamma$	0.99
$K$	128	$m^{max}$	200000
$\eta$	0.9995	$p$	1

- Random: In this setting, the UAV randomly selects the flying direction and distance in each TS. Also, it applies the same optimization method of phase shifts as the DQN-based solution.
- Greedy: In each TS, the UAV moves to the place for maximizing the reward function in Eq. (21). Also, the optimization of phase shifts is the same as the DQN-based solution.

First, we depict the accumulated reward of the proposed DQN-based and DDPG-based algorithm of the training procedure in Fig. 4, where the number of IRSs is set to 3, the number of reflecting elements is 20,  $k_i = 100$ , and  $k_q = 1$ . As shown in Fig. 4(a), the curve of accumulated reward remains negative at the beginning. This is because the UAV may have poor attempts, such as flying out of the target area, resulting in negative reward, i.e, penalty. Additionally, one can see that the accumulated reward increases rapidly at the later stage and the networks start to converge. Eventually, the curve of accumulated reward remain between 15 and 20, which means that the agent has achieved the best options of UAV trajectory and the phase shifts of the reflecting elements. Then, in Fig. 4(b), DDPG also has the similar trend as DQN in Fig. 4(a). Specifically, the curve of the accumulated reward starts to increase from  $-25$  at the beginning. This is because the UAV may fly out of the target area and the penalty is incurred. Then, the learning procedure starts and both actor and critic networks learn to converge, leading to the increase of the accumulated reward. Eventually, one can observe that the curve of accumulated reward remains about 30, which means the networks obtains the best options of trajectory of the UAV and phase shifts of the reflecting elements of IRSs.

Then, we depict the accumulated reward of the proposed DQN-based and DDPG-based algorithm of the training procedure in Fig. 5, where the number of IRSs is set to 6, the number of reflecting elements is 20,  $k_i = 100$ , and  $k_q = 1$ . In Fig. 5(a), we observe that the curve of DQN starts to increase from  $-30$  at the beginning, then it remains between 30 and 40. One can also see that from Fig. 5(b) that the accumulated reward of DDPG finally remains above 40.

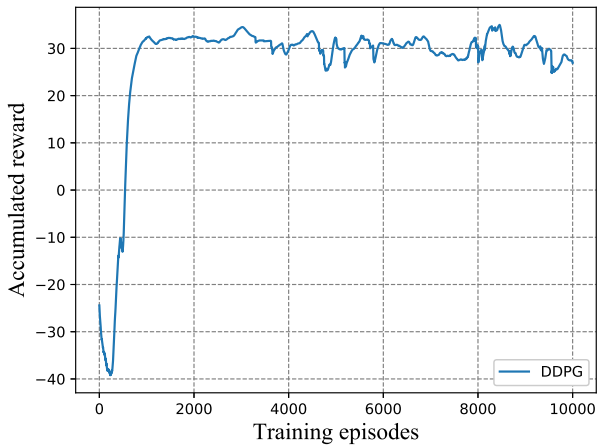




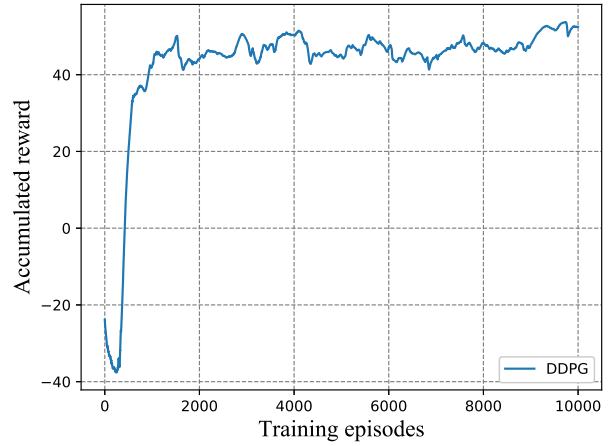
(a)



(a)



(b)



(b)

Fig. 4: Accumulated reward of (a) DQN and (b) DDPG versus training episodes (with 3 IRSs).

Fig. 5: Accumulated reward of (a) DQN and (b) DDPG versus training episodes (with 6 IRSs).

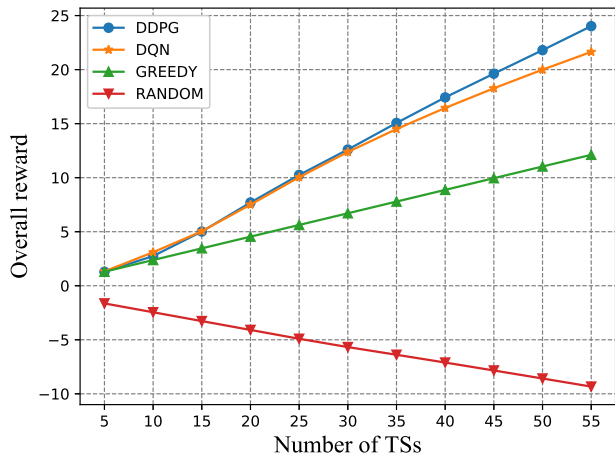
TABLE III: Performance Analysis.

Algorithm	Number of IRSs	Number of TSs	Overall reward
DDPG	3	77	33.36
	6	75	49.58
DQN	3	75	27.38
	6	117	43.43
Greedy	3	104	22.50
	6	104	22.98
Random	3	152	-85.61
	6	157	-85.73

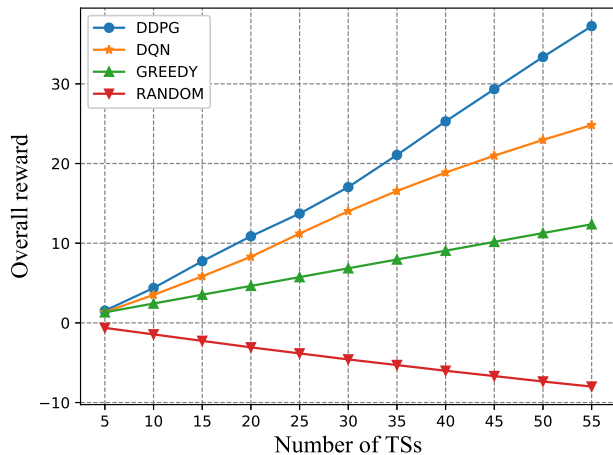
Once the training is done, we can evaluate the performance of the proposed DDPG and DQN-based solutions. In Table III, we show the number of TSs and the overall reward of DDPG, DQN, Greedy and Random solutions that can achieve in one episode. When the number of IRSs is 3, we observe that the UAV controlled by DDPG can serve UEs for 77 TSs, achieving the overall reward of 33.36. Also, DQN can serve UEs for 75 TSs, and achieve the overall reward of 27.38. However, Greedy can only achieve 22.50 of the overall reward, although it can

serve UEs for more TSs. Note that our objective is to achieve the the highest reward, and therefore the number of TSs served is not our first priority. Similarly, when the number of IRSs is 6, we can also observe that DDPG outperforms DQN, Greedy and Random in terms of the overall reward. DQN performs worse than DDPG, as DQN can only have discrete/limited options, but it is more suitable for some practical system with hardware limit. Additionally, one can see that no matter how many IRSs are employed, the overall reward of Random always remains negative. This is because the UAV controlled by Random may always fly out of the target area and achieve the penalty.

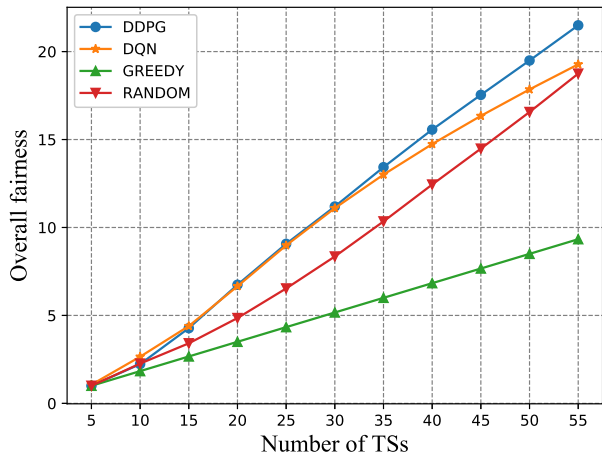
Then, we evaluate the performance in terms of overall reward, fairness, data rate of UEs in different number of TSs in Fig. 6, where the number of IRSs is set to 3. From Fig. 6(a), we analyse the impact of the number of TSs on the overall reward. One observes that as the number of TSs increases, the overall reward of DDPG, DQN and Greedy both increases. Specifically, the DDPG outperforms the solutions of DQN,



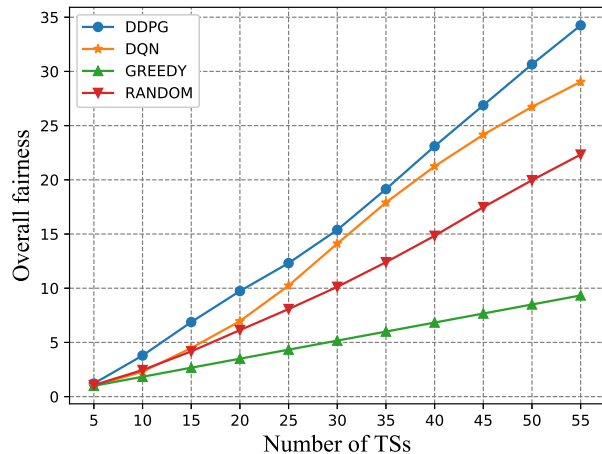
(a)



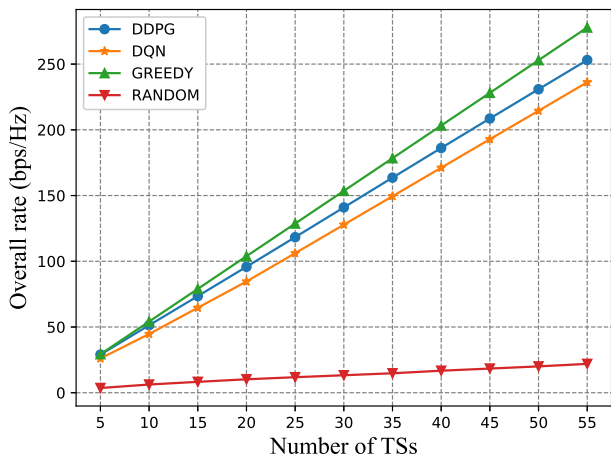
(a)



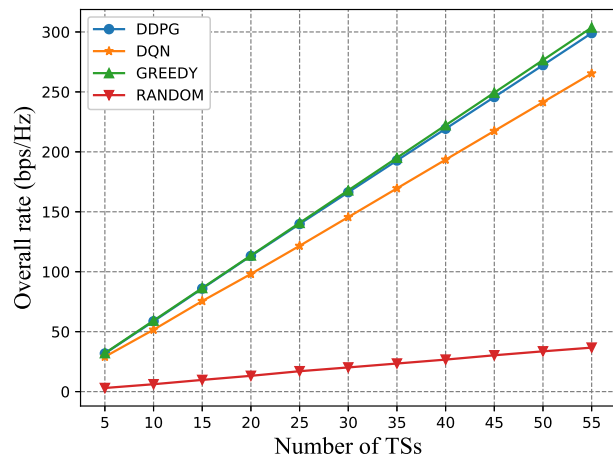
(b)



(b)



(c)



(c)

Fig. 6: The impact of TSs on (a) overall reward, (b) fairness, (c) data rate (with 3 IRSs).

Fig. 7: The impact of number of TSs on (a) overall reward, (b) fairness, (c) data rate (with 6 IRSs).

Greedy and Random, as reasons explained before. Moreover, one can see that Random performs the worst and it decreases with the number of TSs, as no proper control algorithm is applied. In Fig. 6(b), we analyse the overall fairness that DDPG, DQN, Greedy and Random can achieve in different number of TSs. Specifically, one sees that DDPG can achieve better performance than DQN whereas Greedy performs worse than Random. We further analyse the impact of number of TSs on data rate in Fig. 6(c). One observes that Random performs the worst compared to the other benchmark algorithms, as expected. Also, Greedy achieves above 250 bps/Hz, whereas DDPG and DQN perform slightly worse than Greedy. This is because Greedy always controls the UAV fly to the place where it achieves the best data rate, at the cost of fairness. From Fig. 6(b) and Fig. 6(c), one can see that it is quite challenging to achieve the optimal performance of fairness and data rate at the same time. This is because on one hand, the UAV will keep moving to serve different UEs for maximizing the fairness, which will inevitably reduce the data rate and consume more energy of UAV. On the other hand, the UAV will tend to stay at the location that can achieve the maximal data rate, which will have a negative effect on maximizing the fairness.

Furthermore, we depict the performance of overall reward, fairness and data rate of DDPG, DQN, Greedy and Random in different number of TSs in Fig. 7, where the number of IRSs is set to 6. We first compare the overall reward achieved by DDPG, DQN, Greedy and Random in Fig. 7(a). One can see that DDPG achieve the best performance. This is because the proposed DDPG algorithm always tries to find the best UAV trajectory and phase shifts for maximizing the overall reward function. Similarly, DQN has the good performance, which is very suitable for the practical system with hardware limit. The Greedy solution increases with the number of TSs as well and it performs better than Random, as the UAV controlled by Random may fly out of the target area and achieve reward deduction.

Then, as shown in Fig. 7(b), we observe that the fairness of DDPG increases rapidly with the increase of the number of TSs, and it consistently outperforms DQN, Greedy and Random, as expected. Similarly, DQN achieves better performance with the increases of the number of TSs and it eventually remains about 30.

Next, we analyse the performance of DDPG, DQN, Greedy and Random in terms of data rate in different number of TSs in Fig. 7(c). Specifically, Greedy achieves the best performance in terms of data rate, whereas DDPG performs slightly worse than Greedy, as the reason explained before. As expected, one observes that DQN performs worse than DDPG and outperforms Greedy and Random.

Overall, from Fig.7 and Fig. 6, one can conclude that the proposed DDPG and DQN achieve the best balance between fairness and data rate, whereas Random and Greedy cannot balance them.

## VI. CONCLUSION

In this paper, we studied the joint optimization of trajectory of UAV and passive phase shift of reflection elements in an

IRS-assisted UAV communication system, while maximizing the geographical fairness and data rate of all the UEs served by the UAV. We first proposed a DQN-based solution by discretizing the trajectory and phase shift, which has low complexity and is suitable for systems with hardware limits. Then, to tackle the continuous scenario, we have further proposed a DDPG-based solution, which applies to the system where the phase shifts of IRS can be adjusted continuously. The experimental results prove that the proposed solutions achieve better performance compared to other traditional benchmarks.

## REFERENCES

- [1] Y. Zeng, R. Zhang, and T. J. Lim, "Wireless communications with unmanned aerial vehicles: opportunities and challenges," *IEEE Communications Magazine*, vol. 54, no. 5, pp. 36–42, 2016.
- [2] A. Al-Hourani, S. Kandeepan, and S. Lardner, "Optimal LAP altitude for maximum coverage," *IEEE Wireless Communications Letters*, vol. 3, no. 6, pp. 569–572, 2014.
- [3] Q. Wu and R. Zhang, "Common throughput maximization in UAV-enabled OFDMA systems with delay consideration," *IEEE Transactions on Communications*, vol. 66, no. 12, pp. 6614–6627, 2018.
- [4] H. Ren, C. Pan, K. Wang, W. Xu, M. ElKashlan, and A. Nallanathan, "Joint transmit power and placement optimization for URLLC-enabled UAV relay systems," *IEEE Transactions on Vehicular Technology*, pp. 1–6, 2020.
- [5] Y. Zeng, J. Xu, and R. Zhang, "Energy minimization for wireless communication with rotary-wing UAV," *IEEE Transactions on Wireless Communications*, vol. 18, no. 4, pp. 2329–2345, 2019.
- [6] Y. Zeng and R. Zhang, "Energy-efficient UAV communication with trajectory optimization," *IEEE Transactions on Wireless Communications*, vol. 16, no. 6, pp. 3747–3760, 2017.
- [7] C. H. Liu, Z. Chen, J. Tang, J. Xu, and C. Piao, "Energy-efficient UAV control for effective and fair communication coverage: A deep reinforcement learning approach," *IEEE Journal on Selected Areas in Communications*, vol. 36, no. 9, pp. 2059–2070, 2018.
- [8] Z. Yang, C. Pan, K. Wang, and M. Shikh-Bahaei, "Energy efficient resource allocation in UAV-enabled mobile edge computing networks," *IEEE Transactions on Wireless Communications*, vol. 18, no. 9, pp. 4576–4589, 2019.
- [9] W. Huang, Z. Yang, C. Pan, L. Pei, M. Chen, M. Shikh-Bahaei, M. ElKashlan, and A. Nallanathan, "Joint power, altitude, location and bandwidth optimization for UAV with underlaid D2D communications," *IEEE Wireless Communications Letters*, vol. 8, no. 2, pp. 524–527, 2019.
- [10] C. Zhan, Y. Zeng, and R. Zhang, "Energy-efficient data collection in UAV enabled wireless sensor network," *IEEE Wireless Communications Letters*, vol. 7, no. 3, pp. 328–331, 2018.
- [11] C. H. Liu, Z. Chen, and Y. Zhan, "Energy-efficient distributed mobile crowd sensing: A deep learning approach," *IEEE Journal on Selected Areas in Communications*, vol. 37, no. 6, pp. 1262–1276, 2019.
- [12] J. Xu, Y. Zeng, and R. Zhang, "UAV-enabled wireless power transfer: Trajectory design and energy optimization," *IEEE Transactions on Wireless Communications*, vol. 17, no. 8, pp. 5092–5106, 2018.
- [13] T. J. Cui, M. Q. Qi, X. Wan, J. Zhao, and Q. Cheng, "Coding metamaterials, digital metamaterials and programmable metamaterials," *Light: Science & Applications*, vol. 3, no. 10, p. e218, 2014.
- [14] L. Li, T. J. Cui, W. Ji, S. Liu, J. Ding, X. Wan, Y. B. Li, M. Jiang, C.-W. Qiu, and S. Zhang, "Electromagnetic reprogrammable coding-metamaterials holograms," *Nature communications*, vol. 8, no. 1, pp. 1–7, 2017.
- [15] Q. Wu and R. Zhang, "Intelligent reflecting surface enhanced wireless network via joint active and passive beamforming," *IEEE Transactions on Wireless Communications*, vol. 18, no. 11, pp. 5394–5409, 2019.
- [16] K. Wang, Y. Chen, and M. Di Renzo, "Outage probability of dual-hop selective af with randomly distributed and fixed interferers," *IEEE Transactions on Vehicular Technology*, vol. 64, no. 10, pp. 4603–4616, 2015.
- [17] Q. Wu and R. Zhang, "Intelligent reflecting surface enhanced wireless network: Joint active and passive beamforming design," in *2018 IEEE Global Communications Conference (GLOBECOM)*, 2018, pp. 1–6.
- [18] Y. Yang, B. Zheng, S. Zhang, and R. Zhang, "Intelligent reflecting surface meets OFDM: Protocol design and rate maximization," *IEEE Transactions on Communications*, 2020.

- [19] C. Huang, A. Zappone, G. C. Alexandropoulos, M. Debbah, and C. Yuen, "Reconfigurable intelligent surfaces for energy efficiency in wireless communication," *IEEE Transactions on Wireless Communications*, vol. 18, no. 8, pp. 4157–4170, 2019.
- [20] X. Yu, D. Xu, and R. Schober, "Enabling secure wireless communications via intelligent reflecting surfaces," *arXiv preprint arXiv:1904.09573*, 2019.
- [21] G. Zhou, C. Pan, H. Ren, K. Wang, and A. Nallanathan, "Intelligent reflecting surface aided multigroup multicast MISO communication systems," *IEEE Transactions on Signal Processing*, 2020.
- [22] C. Pan, H. Ren, K. Wang, W. Xu, M. Elkashlan, L. Hanzo, and A. Nallanathan, "Multicell MIMO communications relying on intelligent reflecting surfaces," *IEEE Transactions on Wireless Communications*, 2020.
- [23] C. Pan, H. Ren, K. Wang, M. Elkashlan, A. Nallanathan, J. Wang, and L. Hanzo, "Intelligent reflecting surface enhanced MIMO broadcasting for simultaneous wireless information and power transfer," *arXiv preprint arXiv:1908.04863*, 2019.
- [24] T. Bai, C. Pan, Y. Deng, M. Elkashlan, A. Nallanathan, and L. Hanzo, "Latency minimization for intelligent reflecting surface aided mobile edge computing," *IEEE Journal on Selected Areas in Communications*, pp. 1–17, 2020.
- [25] A. Zappone, M. Di Renzo, F. Shams, X. Qian, and M. Debbah, "Overhead-aware design of reconfigurable intelligent surfaces in smart radio environments," *arXiv preprint arXiv:2003.02538*, 2020.
- [26] X. Yu, D. Xu, and R. Schober, "Optimal beamforming for MISO communications via intelligent reflecting surfaces," *arXiv preprint arXiv:2001.11429*, 2020.
- [27] C. Huang, R. Mo, C. Yuen *et al.*, "Reconfigurable intelligent surface assisted multiuser MISO systems exploiting deep reinforcement learning," *arXiv preprint arXiv:2002.10072*, 2020.
- [28] S. Li, B. Duo, X. Yuan, Y.-C. Liang, and M. Di Renzo, "Reconfigurable intelligent surface assisted UAV communication: Joint trajectory design and passive beamforming," *IEEE Wireless Communications Letters*, vol. 9, no. 5, pp. 716–720, 2020.
- [29] D. Ma, M. Ding, and M. Hassan, "Enhancing cellular communications for UAVs via intelligent reflective surface," *arXiv preprint arXiv:1911.07631*, 2019.
- [30] R. S. Sutton and A. G. Barto, *Reinforcement Learning: An Introduction*. Cambridge, MA, USA: A Bradford Book, 2018.
- [31] V. Mnih, K. Kavukcuoglu, D. Silver, A. A. Rusu, J. Veness, M. G. Bellemare, A. Graves, M. Riedmiller, A. K. Fidjeland, G. Ostrovski *et al.*, "Human-level control through deep reinforcement learning," *Nature*, vol. 518, no. 7540, pp. 529–533, 2015.
- [32] T. P. Lillicrap, J. J. Hunt, A. Pritzel, N. Heess, T. Erez, Y. Tassa, D. Silver, and D. Wierstra, "Continuous control with deep reinforcement learning," *arXiv preprint arXiv:1509.02971*, 2015.
- [33] A. G. Barto, R. S. Sutton, and C. W. Anderson, "Neuronlike adaptive elements that can solve difficult learning control problems," *IEEE Transactions on Systems, Man, and Cybernetics*, vol. SMC-13, no. 5, pp. 834–846, 1983.
- [34] D. Tse and P. Viswanath, *Fundamentals of wireless communication*. Cambridge university press, 2005.
- [35] R. K. Jain, D.-M. W. Chiu, and W. R. Hawe, "A quantitative measure of fairness and discrimination," *Eastern Research Laboratory, Digital Equipment Corporation, Hudson, MA*, 1984.